Journal of Graph Algorithms and Applications

http://jgaa.info/

vol. 6, no. 4, pp. 373–404 (2002)

A 6-Regular Torus Graph Family with Applications to Cellular and Interconnection Networks

Mihaela Iridon *David W. Matula*

Southern Methodist University
Computer Science and Engineering Department

mihaela@seas.smu.edu matula@seas.smu.edu

Abstract

This paper introduces a special graph family, together with an extensive characterization of some of its properties and two of its immediate applications. The graph denoted by $T_{i,j,}$ is a regular hexavalent toroidal graph. The topological features of $T_{i,j}$ include vertex symmetry, Hamiltonian decomposition, translation and rotation isomorphism. Topologically, the graph is a torus, while algebraically, it can also be expressed as a Cayley graph, defined on the cyclic group $<1, k, k^2, -1, -k, -k^2>$, where k can be determined from the (i,j) parameters defining graph $T_{i,j}$. As a direct consequence, the proposed graph, which has $\rho_{i,j} = i^2 + i \cdot j + j^2 = (i+j)^2 - i \cdot j$ vertices, is vertex-symmetric. For the special case when $i - j$ is a multiple of 3, the graph has a unique 3-coloring. The diameter of the graph can also be expressed as a function of i and j: $d = \lfloor (2i + j)/3 \rfloor$. As a result of its highly symmetric topology, the graph is employed in modeling and analysis of cellular and interconnection networks. A more appropriate way of modeling highly dense cellular networks is shown to be the model using the triangular lattice in which the nodes represent the transceivers of the network, rather than the traditional hexagonal lattice where coverage overlap regions cannot be explicitly represented. The toroidal embedding of the triangular lattice using the $T_{i,j,}$ graph helps us model and simulate the functionality of a cellular network with strong overlap regions without inducing any artifacts due to boundary effects limitations, simultaneously preserving the regularity of the graph model. For the constructing parameters of $T_{i,j}$, such that $j = i - 1$, the graph is optimal with maximum connectivity and maximum number of vertices for a locally planar graph, given diameter d, which in this case will be equal to j. This feature makes the $T_{i,j}$ graph desirable for interconnection networks topology, together with the graph vertices' algorithmic labeling scheme, presented in this paper.

Communicated by Balaji Raghavachari: submitted May 1999;
revised May 2001 and August 2002.

1 Introduction and Summary

Throughout its evolution, the theory of graphs had placed in the spotlight a relative large number of special graphs with distinctive features and properties, useful in particular application areas or just interesting from the point of view of the graph theoretician. In this context, the main contribution of this paper is the introduction of a special graph, together with a characterization of some of its properties and two of its immediate applications. The graph denoted by $T_{i,j}$ is a regular triangulated toroidal graph and is characterized by remarkable properties such as Hamiltonian decomposition, translation and rotation isomorphism, and features two special cases with interesting coloring and vertex set cardinality properties.

The paper is organized around six sections. In the next section, we introduce homomorphic repeat patterns on the infinite triangular lattice and we describe the construction of the $T_{i,j}$ graph. Its properties are given in Section 3. Section 4 briefly describes some coloring issues and the computation of the diameter of $T_{i,j}$. In Section 5, we give a succinct presentation of the two applications of the regular toroidal graph: cellular and interconnection networks modeling. The proposed graph's highly symmetric structure, high connectivity, and the interaction between the topological and combinatorial properties, confer upon T_{ij} a rich set of properties, which makes it a desirable tool for modeling and simulating various network topologies. Due to its finiteness as well as its regularity-preserving structure, the graph model can be employed in cellular network simulations without inducing any boundary artifacts, in order to model metropolitan area cellular networks with strong overlap coverage regions. We conclude the paper with a summary of results in Section 6.

2 Homomorphisms of the Infinite Triangular Lattice and Graph $T_{i,j}$

2.1 The Infinite Triangular Lattice and Rhombic Numbers

There are three basic regular infinite lattices: the triangular (6-regular), the rectangular (4-regular), and the hexagonal (3-regular) lattice. A planar (2D) rectangular lattice, also referred to as the *2-lattice*, [Hara72] is a graph whose points are ordered pairs of integers (i,j) where $i = 0, 1, \ldots$ and $j = 0, 1, \ldots$. Two of these points are adjacent whenever their distance in the Cartesian plane is 1. In a similar way, we can define the 2D triangular lattice. Even if there are 3 distinct directions $\vec{x}, \vec{y}, \vec{z}$ in the triangular lattice, it is obvious that only two are independent, such that any point is uniquely identified by its (x,y) coordinates. Then, two points $P_1(x_1,y_1)$ and $P_2(x_2,y_2)$ are adjacent iff one of the following conditions hold:

$$\begin{array}{lllll} \text{(i)} & x_1 = x_2 & \text{and} & |y_1 - y_2| = 1 \\ \text{(ii)} & y_1 = y_2 & \text{and} & |x_1 - x_2| = 1 \\ \text{(iii)} & |x_1 - x_2| = 1 & \text{and} & |y_1 - y_2| = 1 \end{array}$$

The infinite triangular lattice is an infinite regular graph of degree 6. Each vertex is adjacent to 6 other vertices and 6 edges, each edge is adjacent to 2 vertices, and each face, which is an equilateral triangle, is adjacent to 3 vertices. Moreover, the infinite triangular lattice is the dual graph of the infinite hexagonal lattice. This is shown in Figure 1, and it represents an interesting observation for the application of this graph in the modeling of cellular networks. In both graph model cases the vertices of the triangular lattice represent centers of the broadcasting regions. However, only the triangular lattice can explicitly show transceiver coverage overlap regions, whereas the hexagonal lattice does not. Moreover, the duality of the two lattices allowed us to build cellular network models of same capacity, in terms of number of channels available and same geographic coverage, however with different number of transceivers. As shown in Figure 1, nodes in the dual graph generating the triangular faces, identify faces (hexagons) in the hexagonal lattice.

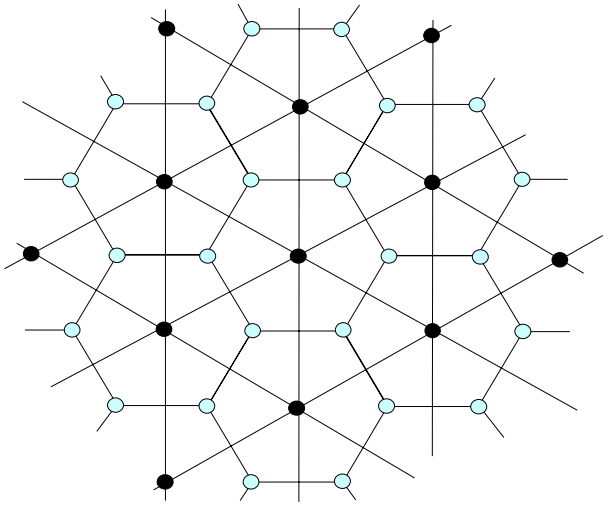

Figure 1 The infinite hexagonal lattice and its dual graph, the infinite triangular lattice

As Arnaud had shown in [Arna80], the regular lattice represents a powerful tool to achieve an efficient use of the frequency spectrum when assigning channels to broadcasting stations. Cellular networks consist of groups of cells serving as a region. Each cell is assigned a set of radio frequency channels and has to deal with calls that either originated within that cell or is a handoff call. A handoff call (also known as a handover call) occurs due to the mobility of the users as well as the load balancing implementations that transfer calls between cells. The number of frequency channels constitutes a limited resource and, moreover, the assignment of channels to geographical cells and regions has to follow certain distance

constraints due to possible interference. Therefore it is necessary to reuse the allocated frequency channels within the network service area to support as many users as possible.

In trying to find a simple algebraic algorithm for cellular layout in the case of hexagonal cellular network models, MacDonald introduced the idea of *shifting parameters* [MacD79]. A year later, Arnaud used the same concept and applied it for frequency planning in triangulated broadcasting network models. He extended this idea and used the notion of *rhombic numbers* defined by the two shifting parameters [Arna80].

Let us consider the infinite triangular lattice and a coordinate system (x,y) with axes offset at 60^0, and with the x-axis along the horizontal direction. Also, let us define along each direction two parameters, i and j, called the *shifting parameters*. They represent graph distances along the x and y axes, accordingly. With i,j given, such that $1 \le j < i$ and i,j relatively prime (i.e., GCD$(i,j) = 1$), we denote the *rhombic number* $\rho_{i,j}$ by the following formula:

$$\rho_{i,j} = i^2 + i \cdot j + j^2 = (i + j)^2 - i \cdot j \qquad (1)$$

Given these parameters, one can place *origin repeat* points on the infinite triangular lattice, as shown in Figure 2, for $i = 3$ and $j = 1$. By connecting the repeat points as depicted in the figure, we obtain a rhombic tiling of the infinite triangular lattice. Arnaud used the idea of rhombic tiling in his paper mentioned earlier, and it emerged as a solution to the problem of covering a given area in the plane with transmitters given a limited number of available channels and considering the distance constraint to avoid interference. The two shifting parameters, i and j, have to be relatively prime because otherwise, the rhombus given by these parameters can be decomposed into non-trivial sub-rhombii. This is desirable because we aim to identify a unique labeling algorithm for the vertices of a region consisting of distinct sets of frequency channels, where the labeling will then identify these sets. Transceivers are situated at the vertices of the underlying

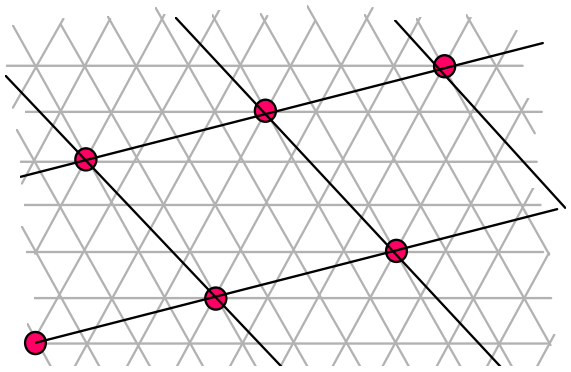

Figure 2 The rhombic tiling of the triangular lattice for shifting parameters i=3 and j=1.

triangular lattice but all the sets of distinct frequencies are within a delimiting rhombus. In Figure 2, the enlarged nodes of the rhombic lattice represent repeating (or identical) sets of voice channels, and the edge of such a rhombus denotes thus the minimal distance for which interference would be avoided.

2.2 Tilings of the Infinite Triangular Lattice

The rhombic tiling, given the shifting parameters *i, j*, is given in Figure 3. The following lemmas will help us identify the number of vertices, edges, and triangular faces covered by a region delimited through a given tiling, and show the equivalence of the presented tilings.

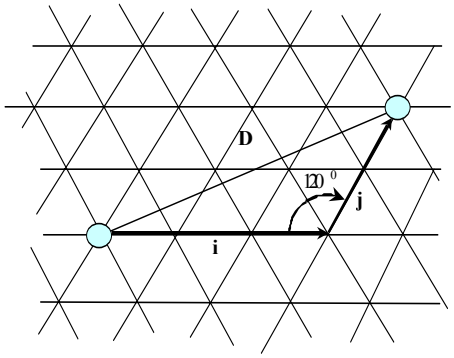

Figure 3 Two repeat origin points at distance D, and shifting parameters (*i*,*j*)

Lemma 1. The side of the rhombus tile is equal to $\sqrt{\rho_{i,j}}$, where (*i*, *j*) are the shifting parameters, and $\rho_{i,j}$ is the rhombic number.

Proof: Given *i* and *j*, the minimum distance between any two repeat-origin points, denoted by *D*, is computed from the triangle outlined in Figure 3 by applying Pythagoras' generalized theorem:

$$D^2 = i^2 + j^2 - 2 \cdot i \cdot j \cdot \cos(120^\circ) = i^2 + j^2 - 2 \cdot i \cdot j \cdot \left(-\frac{1}{2}\right)$$

$$\Rightarrow \quad D^2 = i^2 + j^2 + i \cdot j = \rho_{i,j}$$

□

Lemma 2. The number of vertices contained by the rhombus tile constructed on the infinite triangular lattice with shifting parameters (*i*,*j*), including the corner (origin-repeat) vertex only once, is equal to $\rho_{i,j}$.

Proof: Let the triangular lattice be composed of equilateral triangles of side 1, i.e., $d = 1$. Also, let the side of the rhombus be *D*. The area of an

elementary triangle in the lattice is $A_{triangle} = \frac{\sqrt{3}}{4}$ and the area of the rhombus is $A_{rhombus} = \frac{\sqrt{3}}{2} D^2$.

Given the shifting parameters *i, j*, and applying Lemma 1 we have:

$$A_{rhombus} = \frac{\sqrt{3}}{2} D^2 = \frac{\sqrt{3}}{2} \rho_{i,j}.$$

Thus, the number of triangles inside the rhombus is equal to:

$$N_t = \frac{A_{rhombus}}{A_{triangle}} = \frac{\frac{\sqrt{3}}{2} \rho_{i,j}}{\frac{\sqrt{3}}{4}} = 2 \cdot \rho_{i,j}.$$

Since every triangle is adjacent to three vertices and each vertex is adjacent to six triangles, we can write $2 \cdot |V| = 2 \cdot N_v = N_t$, where N_v and N_t represent the number of vertices and the number of triangular faces, respectively.

Hence, the number of vertices inside the rhombic tile is:

$$|V| = N_v = \frac{N_t}{2} = \rho_{i,j} \qquad \square$$

A special case of pseudo-rhombic tiling, or *degenerate* tiling, given the rhombic number $\rho_{i,j}$, is the *stripe*, where all the $\rho_{i,j}$ vertices are placed on a horizontal line. The surface is delimited by a contiguous series of triangles situated above the points. This is shown in Figure 4, for the case $\rho_{i,j} = 7$.

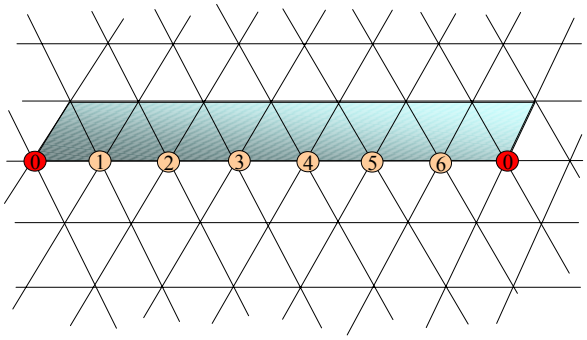

Figure 4 A stripe tiling with 7 vertices and 14 triangles

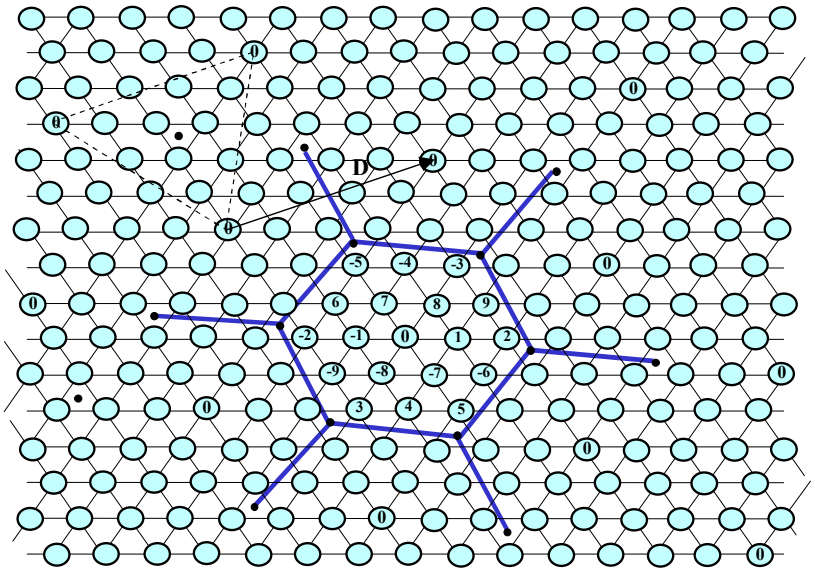

Figure 5 A hexagonal tile with 19 vertices constructed with the Voronoi diagram method. The repeat origin points labeled 0 are at i=3, and j=2.

The darkened points, labeled **0**, denote repeating points. The area of the stripe is the same as the area of a rhombus with the same number of vertices, i.e. with the same number of triangles.

The last and most interesting type of tiling is the hexagonal tiling. If we consider the infinite triangular lattice with the origin repeat points placed at positions given by the shifting parameters (i,j), one can identify a triangulated tiling derived from the rhombic tiling by drawing also the short diagonal of all rhombii. If for each such triangle (half rhombus) we determine the center, we obtain a lattice of points. This is known as the Voronoi diagrams technique [Fort92], and it identifies a cluster of vertices that are closer to a repeat origin point than to any other origin point. The collection of these clusters forms a hexagonal tiling in the triangular lattice. Such a cluster is shown in Figure 5. The hexagonal tile (cluster) represented here contains 19 vertices and the origin repeat points are i=3, j=2. Thus, the rhombic number for this case is $\rho_{3,2} = 19$. A generic triangle (half rhombus) and its center are represented in the left upper corner with a dotted line.

Lemma 3. The hexagonal tile constructed with shifting parameters (i,j) contains $\rho_{i,j}$ vertices.

Proof: In the hexagon depicted in Figure 5, the distance from its center labeled **0** and any of its 6 corners (black dots) is equal to 2/3 of the median

of the generic triangle depicted with a dotted line, since the hexagon corners represent centers of triangles.

Let us denote this distance by R (R is the radius of the hexagon, i.e., the radius of the circumscribed circle). Since each dotted triangle is equilateral (because the origin repeat points are equidistantly placed), the side of such a triangle is equal with the side of the rhombus for the same given deployment.

Hence, we have

$$R = \frac{2}{3} \cdot \left(D \frac{\sqrt{3}}{2} \right) = D \frac{\sqrt{3}}{3} .$$

From this, if we divide the hexagon in 6 equilateral identical triangles by drawing the 6 radii from the center to the 6 corners. Now, we can compute the area of the hexagon as follows:

$$A_{hexagon} = 6 \cdot \left(\frac{1}{2} \cdot R^2 \frac{\sqrt{3}}{2} \right) = 6 \cdot \left(\frac{1}{2} \cdot \left(D \frac{\sqrt{3}}{3} \right)^2 \cdot \frac{\sqrt{3}}{2} \right) = \frac{\sqrt{3}}{2} D^2 .$$

Thus, $A_{rhombus} = A_{stripe} = A_{hexagon} = D^2 \frac{\sqrt{3}}{2}$, and $|V| = \rho_{i,j}$. □

2.3 Toroidal Embeddings. Homomorphism.

The infinite triangular lattice has the important feature of being regular. This property makes it useful in applications such as interconnection and telecommunication networks. But in both cases one cannot perform modeling and simulation techniques because the lattice model is not finite. To preserve the regularity and still obtain a finite regular graph of degree 6, we take a finite region from the infinite triangular lattice, in this case the hexagonal tile from Figure 5, and embed it on a toroidal surface. Thus, the resulting graph is a regular triangulated toroidal graph.

The embedding of a hexagonal shape on a torus is shown in Figure 6, as it is not a trivial operation. (The left identified triangle of the hexagon will be cut and pasted as the triangle on the top-right of the hexagon, and the triangle bottom-right will be cut and pasted as the top-left triangle, hence forming a rhombus which then can be embedded on a torus as shown in the figure to the right.) One can see that it is not evident the fact that the graph is toroidal if looking at Figure 9, as compared to Figure 8, representing the same graph. Moreover, the figure shows that the $T_{i,j}$ graph is not simply a triangular mesh wrapped around a doughnut.

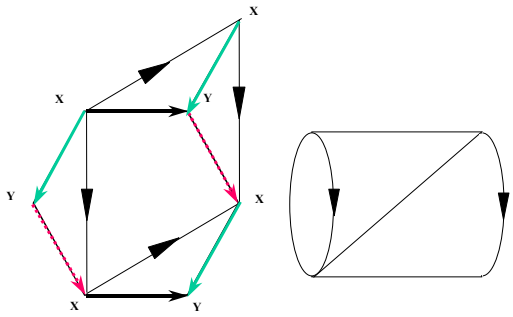

Figure 6 The embedding of a hexagonal surface on a torus by cutting and pasting.

Suppose now, for example. that a generic node a from a given tile is adjacent to a set of nodes $A = \{a_1, a_2, .., a_6\}$, some from the same tile as a and others from one or two adjacent tiles in the lattice. Then, after embedding the tile on a torus, node a will be adjacent to the same set of vertices. For example, in Figure 5, the node labeled -5 is adjacent to the nodes labeled -6, 2, and 3 in other tiles. In the finite toroidal graph, the node labeled -5 is adjacent to the nodes labeled -6, 2, and 3 in the same tile

By embedding a finite repeat pattern (cluster) from the infinite triangular lattice on a torus, we defined in fact a mapping of all the clusters forming the lattice into a generic cluster. In other words, this represents a *many-to-one* mapping, in which all the nodes from the infinite triangular lattice map into the nodes of the toroidal graph. This introduces the notion of *direct homomorphism*, which is different from the notion found in [Hara72].

Definition: A $(direct)$ $homomorphism$ of a given graph G onto G' is a many-to-one mapping, φ, such that if two vertices labeled u and v are adjacent in G, then φu and φv are adjacent in G'. (Note that in G multiple distinct vertices may share the same label.)

Both cases described in the previous section, the rhombus and the hexagon embedded on a torus, represent homomorphisms of the infinite triangular lattice. Adjacency is preserved, and as a consequence, regularity is also preserved. Hence, every vertex of the infinite triangular lattice maps onto the vertex set of the finite toroidal triangulated graph.

2.4 The Generation of $T_{i,j}$

The following algorithm describes the labeling of the vertices, as depicted previously in Figure 5. The labeling scheme is a major contribution of this paper in the area of cellular networks and its practical importance will be discussed later.

The Labeling Algorithm ($T_{i,j}$ Generation)

Step 1: Place the origin repeat vertices, labeled with 0, at offsets of i steps on the horizontal x-axis and j steps on the 60^0 skew (counterclockwise) y-axis.

Step 2: Label the vertices on every x-axis between repeat points with values:

$$0,1,2,\ldots,\left\lfloor \frac{\rho_{i,j}}{2} \right\rfloor,-\left\lfloor \frac{\rho_{i,j}}{2} \right\rfloor,\ldots,-2,-1,0 \cdot$$

Step 3: Using the Voronoi diagrams, identify the hexagonal tiling.

Step 4: Pick any tile and wrap it on a toroidal surface, preserving adjacency according to the direct homomorphism definition. The regular toroidal graph obtained, given the two shifting parameters (i,j), is denoted by $\boldsymbol{T}_{i,j}$.

The labeling scheme uses a symmetric residue numbering [HaWr79]. In Figure 5, the hexagonal tile (obtained from Steps 1 and 2 in the algorithm above) contains 19 vertices, labeled –9, –8 … –1, 0, 1… 8, 9. Notice that in this case, the shifting parameters were (3,2) yielding the rhombic number 19, equal to the number of vertices, as also shown in Lemma 3.

It is important to note here that the above labeling scheme implies the actual drawing and geometrical identification of the hexagonal tile that defines the graph. However, there exists a direct relationship between any two adjacent vertices, and this relationship defines, as we shall see later in Lemma 6, the Hamiltonian decomposition of the graph. Two nodes i and j are adjacent in $\boldsymbol{T}_{i,j}$ if one of the following holds:

$$\mathrm{j} = (\mathrm{i} \pm 1) \ mod_{\mathrm{r}} \ \rho_{i,j},$$

$$\mathrm{j} = (\mathrm{i} \pm k) \ mod_{\mathrm{r}} \ \rho_{i,j},$$

$$\mathrm{j} = (\mathrm{i} \pm k^2) \ mod_{\mathrm{r}} \ \rho_{i,j},$$

where $\boldsymbol{mod}_r$ refers to the residual modulo function (see the definition given with Lemma 6). The constant denoted by k can be computed from the parameters of the graph, i and j, as shown below. The value of k is actually the value of the label on the vertex that is adjacent to the origin-repeat point along the positive direction of the y-axis.

The Computation of k, given i and j.

If we start from a given origin point labeled 0 on the infinite lattice, one needs to go an integer number of steps of i and j until it reaches the next closest origin repeat point that is located on the horizontal line below the starting point. This is shown in Figure 7. This is so because we want to reach in straight line the first vertex labeled k, i.e., the vertex adjacent to the

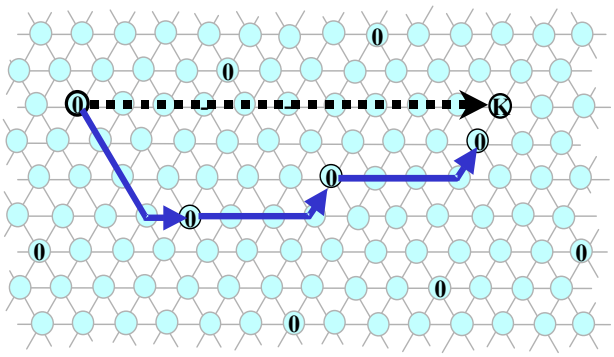

Figure 7 The graphic scheme for the computation of k

origin in the positive direction of the y-axis. This can be expressed as follows:

$$(x \cdot i) \bmod j = 1 \qquad \text{or}$$

$$x \cdot i - y \cdot j = 1 . \qquad (2)$$

The two unknowns, x and y, in Equation (2) can be determined in a relatively small number of arithmetic operations, using the theory of continued fractions based on the Euclidean GCD algorithm [KoMa85], [MaKo80], [HaWr79].

Otherwise, this can be viewed as an integer programming problem, as formulated below, but which has no linear-time solution algorithm:

$$\begin{aligned} &\textit{minimize} && x + y \\ &\textit{s.t.} && y \cdot j - x \cdot i = 1 \\ & && x, y > 0 \\ & && x, y \in Z \end{aligned}$$

After determining x and y, the constant k can now be calculated using the formula given below:

$$k = \left(j \cdot x + i \cdot (x + y)\right) \bmod_r \rho_{i,j} \qquad (3)$$

The following gives direct computation formulas for the constant k in some particular cases.

Case 1: j=1. In this case, it is obvious that going only i steps to the left on the x-axis, we reach the closest vertex labeled k. Hence, for $T_{i,1}$, $k = -i$.

Case 2: j=2. Since GCD(i,j)=1, one needs to go i *div 2* steps down the y-axis, after going once j=2 steps down the z-axis. This means that $k = \left\lceil \frac{i}{2} \right\rceil \cdot i + j$.

Case 3: j=3. Following the same reasoning, and splitting into two sub-cases for $i = 3 \cdot m_1 + 1$, and $i = 3 \cdot m_1 + 2$, for some integer m_1, the constant k is:

$$k = \left\lceil \frac{i}{3} \right\rceil \cdot i + 3, \qquad \forall i = 3m_1 + 1, m_1 > 0$$

$$k = -\left(\left(\left\lceil \frac{i}{3} \right\rceil + 1 \right) \cdot i + 3 \right), \qquad \forall i = 3m_1 - 1, m_1 > 1$$

The above two formulas can be merged into one, such that

$$k = \text{sign}\,(i \bmod_r j) \cdot \left(\left(\left\lceil \frac{i}{3} \right\rceil + \frac{1 - \text{sign}(i \bmod_r j)}{2} \right) \cdot i + j \right), \qquad (4)$$

where sign(x) is the sign function.

Formula (4) holds also for the case j=2 if the first term in the parenthesis is replaced by $\left\lceil \frac{i}{j} \right\rceil$. However, a more general formula, covering all cases of j, could not be identified.

Case 4: j=i–1. This is a special case that will be presented in more detail in the next chapter. Here, the constant k is simply $(3i–1) mod_r \rho_{i,j}$. (The residual modulo is needed only for the minimal case of $T_{2,1}$, which is an isolated case with $k < 0$. Moreover, $T_{2,1}$=K_7.)

3 Properties of the $T_{i,j}$ Graph Family

Lemma 4. Graph $T_{i,j}$ has $\rho_{i,j}$ vertices, $2\rho_{i,j}$ triangular faces, and $3\rho_{i,j}$ edges.

Proof: The first statement regarding the number of vertices in $T_{i,j}$ has been proven in Lemma 3. Since each vertex in the graph is adjacent to 6 triangles and each triangle is adjacent to 3 vertices, the number of triangular faces is 6/3=2 times the number of vertices: $|F| = 2|V| = 2 \cdot \rho_{i,j}$. Moreover, since each vertex in the graph is adjacent to 6 edges and each edge is adjacent to 2 vertices, the number of edges in the graph is 6/2=3 times the number of vertices: $|E| = 3|V| = 3 \cdot \rho_{i,j}$. □

Lemma 5. Graph $T_{i,j}$ is vertex transitive, where the automorphism $\alpha_V: V(T_{i,j}) \to V(T_{i,j})$, mapping vertex p into vertex q, for $-\left\lfloor \frac{\rho_{i,j}}{2} \right\rfloor \le p < q \le \left\lfloor \frac{\rho_{i,j}}{2} \right\rfloor$, adds $(q-p) \bmod_r \rho_{i,j}$ to each vertex label.

Proof: According to the definition, a graph G is vertex transitive if for every pair $p, q \in V(G)$ there is an automorphism that maps p into q. Such a mapping is given above and we only need to show that the graph before the mapping is isomorphic to the one obtained after the mapping.

For this reason, it is sufficient to prove that, since p will map into q, the adjacent vertices to p before the mapping will become, after the translation, the adjacent vertices to q as of before the mapping. Applying the α_V transformation to the 6 neighbors of p, we obtain:

$$\begin{aligned}
\alpha(p+k) &= (p+k)+(q-p) = q+k \\
\alpha(p+k-1) &= (p+k-1)+(q-p) = q+k-1 \\
\alpha(p-k) &= (p-k)+(q-p) = q-k \\
\alpha(p-k+1) &= (p-k+1)+(q-p) = q-k+1 \\
\alpha(p+1) &= (p+1)+(q-p) = q+1 \\
\alpha(p-1) &= (p-1)+(q-p) = q-1
\end{aligned}$$

The above is valid for any vertex p in the graph. Hence, $T_{i,j}$ is vertex-transitive, with the automorphism mapping specified as above. □

Observation: Since the graph is also a Cayley graph, it is inherently vertex-transitive or vertex-symmetric [Aker89]. In certain applications, such as interconnection networks, the vertex-symmetry is an important property because it implies that every node (processor) in the network can be mapped into any other node. In other words, the network/graph looks the same from each node/vertex.

Lemma 6. Graph $T_{i,j}$ factors into three Hamiltonian cycles, given by:

$$\begin{aligned}
&0,1,2,\ldots,\left\lfloor \frac{\rho_{i,j}}{2} \right\rfloor,-\left\lfloor \frac{\rho_{i,j}}{2} \right\rfloor,\ldots,-2,-1,0 \\
&0,k,2k,3k,\ldots,(\rho_{i,j}-1)k \pmod{\rho_{i,j}}_r \\
&0,k^2,2k^2,\ldots,(\rho_{i,j}-1)k \pmod{\rho_{i,j}}_r
\end{aligned}$$

where k is the label value adjacent to the origin in the y-direction. The function $\bmod_r$ refers to *the residual modulo function*, defined as follows:

$$a \bmod_r b = \begin{cases} a \bmod b & \text{if } a \bmod b \le \left\lfloor \frac{b}{2} \right\rfloor \\ (a \bmod b) - b & \text{if } a \bmod b > \left\lfloor \frac{b}{2} \right\rfloor \end{cases}$$

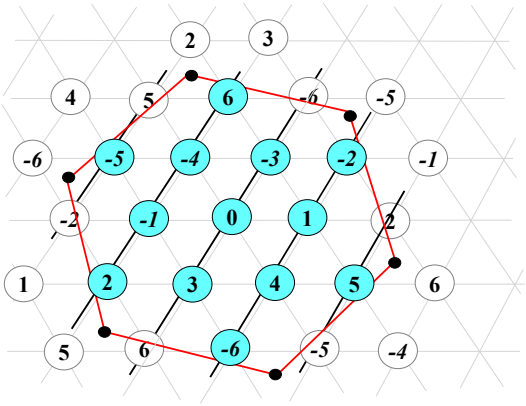

Figure 8 The Hamiltonian cycle along the y-axis, for $T_{3,1}$ with 13 vertices.

Proof: The Hamiltonian cycle along the y-axis can be identified in Figure 8. The complete Hamiltonian decomposition is shown in Figure 9, for the same graph $T_{3,1}$ but drawn in a different fashion, to help visualizing the 3 edge-disjoint cycles. It is obvious that along the x-direction (in Figure 8), the labels in the sequence of vertices along the Hamiltonian cycle are incremented by 1, because of the construction of $T_{i,j}$ itself.

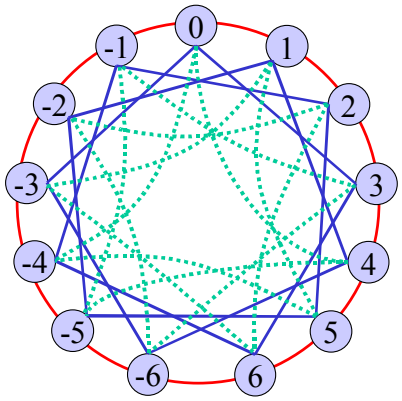

Figure 9 The $T_{3,1}$ graph with its Hamiltonian decomposition

Along the *y*-axis, suppose that we look at the first two vertices from the origin repeat point along the positive direction of the *y*-axis. The vertex adjacent to the origin is labeled *k*. According to the vertex-transitivity lemma, if we map vertex 0 into *k*, then *k* will map into $(k+(k-0))\bmod_r \rho_{i,j}$, which is equal to $(2k)\bmod_r \rho_{i,j}$. This implies that moving along the positive direction of the *y*-axis in increments of one, we add *k* to the labels of the vertices. Likewise, moving along the negative direction of *y*, we subtract *k*, but always applying the residual modulo function to the resulting label.

Following the same reasoning as when determining the constant *k*, we now try to determine the constant *k'*, which corresponds to the adjacent vertex to the origin along the positive direction of the *z*-axis. This is in actuality the vertex *k*-1, but now we try to prove that $k-1=k^2$. Thus, staring from the origin and going up the *y*-axis, one has to jump $x \cdot j + y \cdot (i + j) + 1$ steps to reach the first label *k'*. But each jump represents an addition by *k* to the vertex label. Now, since $i \cdot x = j \cdot y + 1$, from (2), the number of steps in the formula above is equal to *k*. Hence, the vertex *k'* has a label value of $(x \cdot j + y \cdot (i + j) + 1) \cdot k = k^2$. This implies that going along the positive direction of the *z*-axis, one can either add the value (*k*–1) to the vertex labels, or add k^2. This explains the quantity added to the labels of the vertices in the third Hamiltonian cycle. Note that all three Hamiltonian cycles are edge disjoint since each follows a different direction. Moreover, since each cycle has a length of $\rho_{i,j}$, equal to the number of edges/vertices in the cycle, and since all three cycles are edge disjoint, they form a 2-factorization of $T_{i,j}$ [Hara72]. □

Observation: Hamiltonian decomposition implies maximum connectivity and maximum fault tolerance — properties of central importance in interconnection networks. The $T_{i,j,}$ graph is 6-regular and due to the Hamiltonian decomposition, it is characterized by 6 edge-disjoint paths between any two nodes in the graph. Hamiltonian decomposition has been a central area of research not only in graph theory and algebraic topology, but also in communication algorithms for interconnections networks, and even physics. An abundance of papers can be found, as early as the forties, and substantially increasing during the late 80s and mid 90s. To mention just a few names: V. Chvatal [Chva85], P. Erdos [ChEr72], B. Bollobas [BoEr76, Boll79], T.W. Tillson [Till80], C. Thomassen [Thom80], J. Sibeyn [SiKa94], and many others.

Lemma 7. Graph $T_{i,j}$ has an isomorphism corresponding to a 60^0 counterclockwise (geometric) rotation obtained by multiplying each label by the constant *k*, reduced modulo $\rho_{i,j}$. It follows that $k^6 \equiv 1 \bmod_r \rho_{i,j}$.

Proof: As shown in Lemma 6, going in the positive direction of the *y*-axis, one has to add the value *k* to the labels, and going in the positive direction of

the z-axis, the value to be added is k^2. This proves that the vertex labeled k will map into k^2 after a 60^0 rotation counterclockwise. That is, the rotation mapping is to multiply the vertex label by k. Applying a series of such rotations, vertex k^2 will map into vertex $k^3=-1$, k^3 maps into $k^4=-k$, k^4 maps into $k^5=-(k-1)$, and finally, k^6 maps back into the vertex labeled 1. To show that the rotated graph is isomorphic to the initial graph, a similar reasoning, based on the computation of the adjacent vertices, as presented in Lemma 4, can be used. □

Observation: The above rotation mapping is actually a cyclic automorphism of the group T_{ij} defining the (Cayley) graph. Given the generators of the group S = <1, k, k^2> and their inverses (as defined by the group operation): <–1, –k, k^2>, then the rotation automorphism, ω, will map $\omega(s_i) = s_{i+1}$. Since graph $T_{i,j}$ is a Cayley graph, and given it has a cyclic automorphism, we have that $T_{i,j}$ is *rotational* [Heyd97a]. Moreover, $T_{i,j}$ admits a *complete rotation*. This property could be very useful to derive optimal algorithms for interconnection networks, such as broadcasting and gossip algorithms [Heyd97b]. However, not all Cayley graphs are rotational, such as the cube-connected cycles, which are non-rotational Cayley graphs.

Lemma 8. Graph $T_{i,j}$ is edge-transitive, with the automorphism α_E: $E(T_{i,j}) \rightarrow E(T_{i,j})$, mapping edge p_1q_1 into edge p_2q_2 determined by additions and multiplications on all labels.

Proof: The automorphism mapping one edge into any other edge is described by the following steps:

Step 1: First, since the graph is vertex-transitive, the vertex p_1 will be translated in the origin according to the mapping α_V, by subtracting from every vertex label the value p_1 reduced modulo $\rho_{i,j}$. Now p_2 becomes $p_2' = (p_2 - p_1) \bmod_r \rho_{i,j}$. Similarly, we obtain q_2', q_1' and, of course, $p_1' = 0$.

Step 2: Next, we perform a finite number of rotations, since the graph has a rotation isomorphism of 60^0. To determine the number $n \in \{0,..,5\}$ of counterclockwise rotations needed, one has to solve the following equation: $k^n \cdot ((q_1' + p_2') \bmod_r \rho_{i,j}) = q_2' \bmod_r \rho_{i,j}$. It is as if we intend to map first the vertex p_1' into p_2' and then see how many rotations are needed to map the new q_1' $(=q_1'+p_2')$ into q_2'. Having determined n, one can now perform n rotations according to α_E by multiplying each vertex label by k^n reduced modulo $\rho_{i,j}$. The new labels are:

$$p_1'' = 0, \quad q_1'' = q_1' \cdot k^n \bmod_r \rho_{i,j},$$

$$p_2'' = p_2' \cdot k^n \bmod_r \rho_{i,j}, \quad q_2'' = q_2' \cdot k^n \bmod_r \rho_{i,j}$$

Step 3: Last, we perform the final translation of p_2 steps, by adding this value to all vertices. The resulting labels are:

$$p_1''' = p_2$$

$$q_1''' = q_1'' + p_2 = ((q_1 - p_1) \cdot k^n + p_2) \bmod_r \rho_{i,j}$$

$$p_2''' = p_2'' + p_2 = ((1 + k^n) \cdot p_2 - p_1) \bmod_r \rho_{i,j}$$

$$q_2''' = q_2'' + p_2 = ((q_2 - p_1) \cdot k^n + p_2) \bmod_r \rho_{i,j}$$

The steps described above represent the edge automorphism mapping. To prove that the graphs, before and after the rotation, are isomorphic, one can follow a similar reasoning as in the case of the vertex-transitivity lemma and compute the new labels of the adjacent vertices of the two edges. This concludes the proof that the graph $T_{i,j}$ is edge-transitive. □

Just as in the case of the rotational isomorphism, not all Cayley graphs are characterized by edge-transitivity, with the same counterexample of the cube-connected cycle networks.

4 Coloring Issues and the Diameter of $T_{i,j}$

4.1 Discussion on the Coloring of $T_{i,j}$

The vertices of graph $T_{i,j}$ cannot be colored with less than 3 colors, since it has a complete sub-graph that is a cycle of length 3, i.e. the triangle. With each vertex having degree 6, the maximum number of colors needed for $T_{i,j}$ is 7 (see Proposition derived from Greedy Coloring Algorithm in [West96]). Except for $T_{2,1}$ which is a clique (K_7), according to [Broo41], the chromatic number χ of a connected graph G of maximum degree $\Delta(G)$, which is not a clique or an odd cycle, satisfies the following: $\chi(G) \leq \Delta(G)$. In our case, we have $\chi(T_{i,j}) \leq 6$.

We will show that for some cases there exists a 3-coloring, whereas for other cases, there exists a 5-coloring.

Case 1: $i-j = 3m_1$, for $m_1>0$

In this case, the number of vertices in the graph is equal to: $i^2 + i \cdot (3m_1 - i) + (3m_1)^2 = 3(m_1 + 3m_1^2) = 3m_2$, for some positive m_2. In the case of the regular triangulated graph, this is a necessary condition for it to have a 3-coloring, because all elementary cycles are of length three (triangles) and no larger.

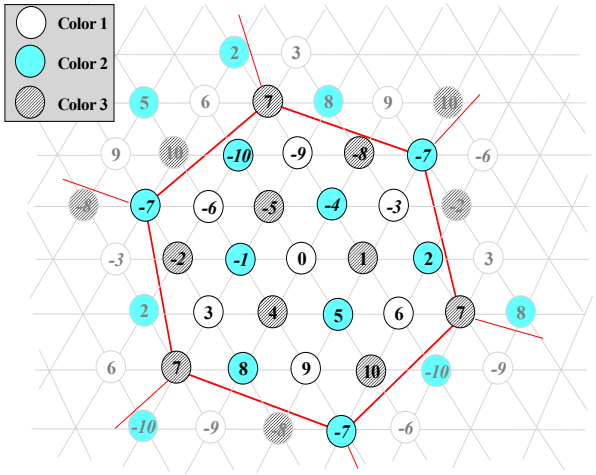

Figure 10 The coloring of $T_{i,j}$ when $i-j=3m$ for $T_{4,1}$

This particular type of graph has all corner vertices of its hexagonal tile representation (see the tilings of the triangular lattice) corresponding to vertices in the infinite triangular lattice. All other $T_{i,j}$ graphs, as the one shown in Figure 5, have the hexagonal corner vertices falling in centers of triangles in the infinite lattice. The two vertices mentioned above are repeating in an interleaved fashion, such that each appears three times at the corners of the hexagonal tile.

An example of this particular case, when $(i\text{-}j)$ mod 3 = 0, together with its unique 3-coloring is given in Figure 10. The graph displayed is $T_{4,1}$ with 21 vertices. Notice that the graph has a multiple-of-three number of vertices. Also, the vertices 7 and -7 (i.e., $\rho_{i,j}/3$ and $-\rho_{i,j}/3$) are the vertices repeating on the corners of the hexagonal tile. The validity of the coloring can be checked by looking at the colors of the vertices with the same label, inside and outside the central hexagonal tile.

Case 2: $i = 2\ ,\quad j = 1$

This case is an exceptional one for graph $T_{2,1}$ and it is the only case when 7 colors are needed. Graph $T_{2,1}$ is the clique on 7 vertices, K_7, and thus has a chromatic number equal to the number of vertices: $\rho_{2,1} = 2^2 + 2 \cdot 1 + 1^2 = 7$.

Case 3: $i > j > 0$ **,** for all i,j with GCD(i,j)=1 not included in Case 1 and Case 2.

In this case, no 3 or 4 coloring has been found. A reason why there is no 3-coloring is because the graph is 6-regular, the length of the smallest cycle is 3, and the number of vertices is not a multiple of 3. Moreover, since the

triangular lattice is uniquely 3-colorable, the triangulated torus in this case cannot have a 3-coloring. A scheme that depicts the compulsion to use 5 colors is shown in Figure 11. Here the first step involves the coloring of the vertices around the 6 corners of the hexagonal tile. There are several possible combinations but no matter what combination we pick, when coloring the rest of the graph as shown in the second step, a fourth, and then a fifth color is necessary. The dotted labels mean that there is a choice to interchange the labels, but the cases are symmetric. The labels A, B, and C suggest the order of picking the colors, and in parentheses are the colors picked for this particular case. All cases are just permutations of the one displayed and one will obtain the same coloring result, i.e. that 5 colors are needed and sufficient for the coloring of the $T_{i,j}$, for i and j not included in the previous two cases.

The coloring of the $T_{i,j}$ graph is employed in the resource allocation problem for interconnection networks, where a limited number of resources need to be uniformly dispersed throughout the network [BaeB97].

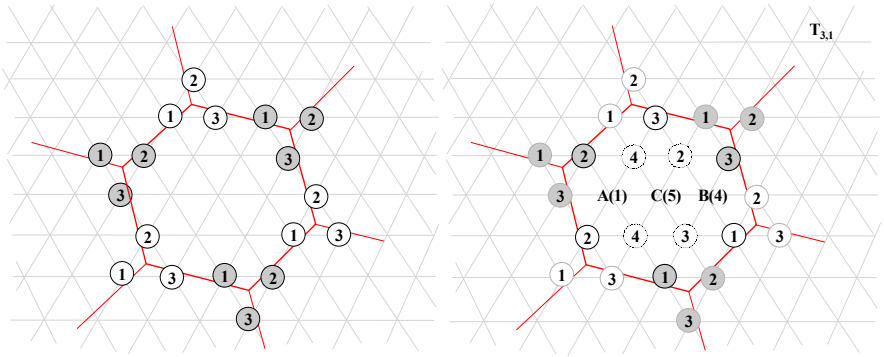

Figure 11 Two steps in the coloring procedure of the general case of $T_{i,j}$

4.2 The Computation of the Diameter of $T_{i,j}$

The diameter of a graph is the length of any longest shortest path between any two vertices in the graph. Let us consider the repeat origin points highlighted on the triangular lattice in Figure 12. The diameter of the T_{ij} graph can then be easily computed as the shortest graph distance from the origin labeled as **A** to the point **P**, which actually represents the physical corner of the hexagon in the hexagonal tiling using the Voronoi diagram, as shown in Figure 5. Note that P could coincide or not with a lattice point, in which case we will take the integral part of the AP distance. Hence,

$$\|AP\| = \frac{1}{3}\|AF\|$$

The *graph distance*, denoted by $d()$, between the points **A** and **F** can be computed using the construction depicted in Figure 12, as follows:

$$\begin{aligned} d(A,F) &= d(A,B) + d(B,F) = \\ &= (d(A,C) - d(B,C)) + (d(C,D) + d(D,E) + d(E,F)) = \\ &= (i - j) + (j + i + j) = \\ &= 2 \cdot i + j \end{aligned}$$

Hence, the diameter of the graph can be expressed, simply, as:

$$d = \left\lfloor \frac{2 \cdot i + j}{3} \right\rfloor \qquad (5)$$

Note: One can obtain the same result by using Euclidean geometry [IrTh99]. However, the proof would be rather lengthy.

4.3 Local Planarity

The $T_{i,j}$ graph is locally planar in the context that given the number of vertices $\rho_{i,j}$ of the graph, then the formula

$$d_0 = \left\lfloor \frac{\sqrt{3}}{2} \cdot \sqrt{\frac{\rho_{i,j}}{3}} \right\rfloor - 1 = \left\lfloor \frac{\sqrt{\rho_{i,j}}}{2} \right\rfloor - 1$$

defines the diameter of the largest induced subgraph of $T_{i,j}$ which is planar [IrTh99]. This subgraph defines a planar hexagonal tile inscribed in the bigger hexagonal (toroidal) tile representing the $T_{i,j}$ graph.

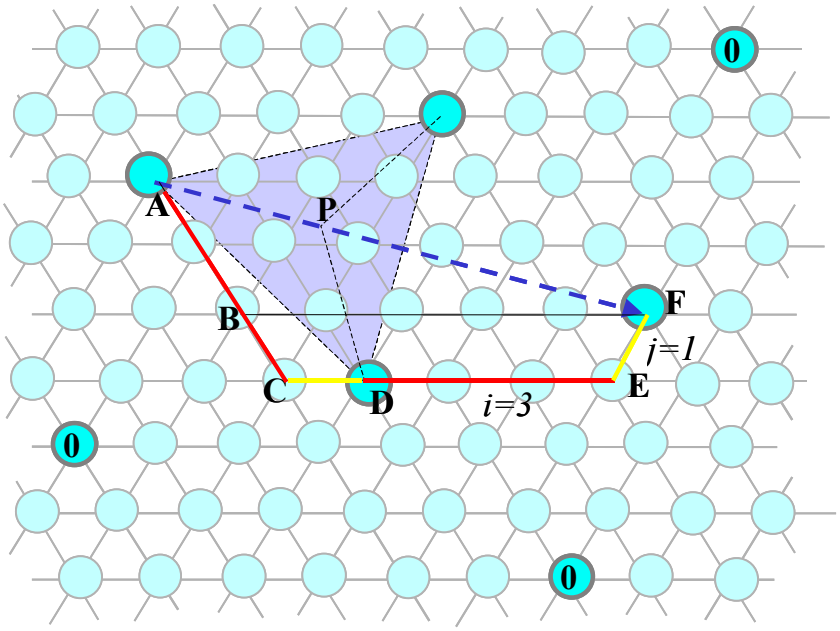

Figure 12 The computation of the diameter

The local planarity property allows us to represent the graph as a hexagon on the infinite triangular lattice, and showing the toroidal embedding along the pasting edges as duplicate nodes around the tile, just as we show the traditional rectangular torus as a rectangular tile embedded in the plane. As we shall see in the following section, the $T_{i,j}$ graph has the maximum number of vertices for a 6-regular graph. This is valid for any 6-regular graph that is embeddable on a surface of genus 1, i.e. the surface of a torus. This fact proved to be helpful in modeling and simulating cellular networks, since we could keep the model finite while preserving its regularity and avoiding undesired and artificial boundary effects. Being able to represent the graph in the plane in this fashion, helped us identify its topological properties, the most important being the fact that $T_{i,j}$ is toroidal.

5 Applications

5.1 The Optimal $T_{i,j}$

If $j = i - 1$, according to (5) the diameter of the $T_{i,j}$ graph becomes $d = i - 1$. The number of vertices is equal to:

$$\rho_{i,j} = 3(i-1)^2 + 3(i-1) + 1 = 3 \cdot d^2 + 3 \cdot d + 1 .$$

We can show by induction that this value represents the maximum number of nodes situated at distance d on the infinite triangular lattice, from any given point, as follows:

Assume the starting point 0. We expand from 0 by determining the number of nodes at distance 1, 2, … from it. Let's denote by $N(d)$ the total number of nodes situated at distance less than or equal to d. Hence:

$$N(0) = 1$$
$$N(1) = 1 + 6 = 7$$
$$N(2) = 1 + 6 + 12 = 19$$
$$\dots$$
$$N(d) = 1 + 6 + 12 + \dots + 6d$$
$$= 1 + 6\sum_{i=1}^{d} i = 1 + 6\frac{d(d+1)}{2} = 3d^2 + 3d + 1$$

Assuming $N(d)$, we need to prove that

$$N(d+1) = 3(d+1)^2 + 3(d+1) + 1 .$$

At distance d we are adding $6(d+1)$ vertices. Then,

$$\begin{aligned} N(d+1) &= N(d) + 6(d+1) \\ &= 3d^2 + 3d + 1 + 6d + 6 \\ &= 3d^2 + 6d + 3 + 3d + 3 + 1 \\ &= 3(d+1)^2 + 3(d+1) + 1 \end{aligned}.$$

This number is maximal because at any step at distance d while expanding from the origin point we cannot add more than $6d$ nodes, since the number of all vertices situated at distance *exactly* d from the point 0 is equal to $6d$. In the context of the maximum number of nodes, given a diameter d, the graph $T_{i,i-1}$ is considered to be optimal. This property is very important especially in the design of interconnection networks where it is desirable to reduce the topological communication latency. Due to the relatively high degree of the graph and its Hamiltonian decomposition mentioned earlier, the $T_{i,j}$ topology offers maximum connectivity and maximum fault tolerance, achieving 6 edge-disjoint paths between any two nodes/processors in the network. Figure 13 shows the smallest optimal $T_{i,j}$, the graph $T_{2,1}$ which has 7 nodes and which, since it is regular of degree 6, it is the clique on 7 vertices, K_7.

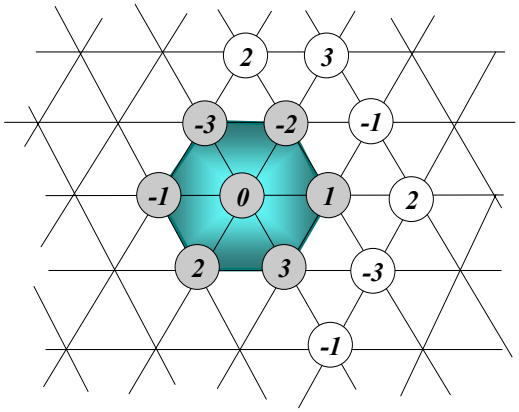

Figure 13 Graph K_7 as the toroidal $T_{2,1}$. The duplicate nodes are represented with light color

5.2 Applications to Interconnection Networks

There is no exact way to compare different topologies of interconnection networks [Sieg96], [Bhuy97], [Mold93]. Still, there are some metrics for interconnection networks and these are useful to take into account when designing new topologies. These features are described below.

Network connectivity: Network connectivity measures the resiliency of a network and is the ability to continue operation despite disabled components. In other words, the connectivity represents the minimum

number of nodes or links that must fail in order to partition the network into two or more disjoint networks (that is, to disconnect the network graph).

Network Diameter: Similar to the diameter definition of a graph, here the network diameter represents the minimum inter-node distance. It can be interpreted as the maximum number of links that must be traversed when sending a message to any node along the shortest path.

Bisection Width: Sometimes it is useful to measure the *congestion* of a network, that is the traffic along the links of the network). It is most useful when designing load-balancing algorithms. The bisection width, or narrowness, of a network can be calculated by partitioning the network into two sub-networks S_1 and S_2, each with N_1 and N_2 processors (with $N_1 \leq N_2$), and determining the ratio between N_1 and the number of links between S_2 and S_1. In fact, this is a *min.-cut max.-flow* type of problem found in network flow theory [FoFu62].

Network Expansion Increments: Another goal that is very important when designing an interconnection network is scalability. It should be possible and easy to scale the network at any time at a user-required size (flexibly), i.e., to add new processors and new links with minimum effort and cost. Also, for cost reasons, it is desirable that the increments are small. This implies the possibility of upgrading the network to the desired size with a given budget.

However, these are only a few characteristics to look at and they are mostly static features of a network but with direct implications in the dynamic behavior of the network.

The wraparound (4-regular) mesh is the most common topologies used in this field, probably because the human mind finds it easy to imagine topologies in a Cartesian coordinate system. Although is expands to higher dimensions, complicating the visualization of the network, the hypercube is another common and well-known topology. Our extensive research in this area showed that only one research group at the University of Michigan, Ann Arbor, designed and implemented a 6-regular interconnection topology [Chen90]. However, the underlying graph (which is the same as the optimal $T_{i,j}$, that is j=i–1) has been employed on a rather empirical basis, without and theoretical justification. Moreover, it has not been shown nor mentioned that the topology is actually a torus, or that a more generalized topology exists, featuring the same properties derived from its symmetric structure.

The optimal $T_{i,j}$ is useful in the area of interconnection networks not only for its maximum connectivity and maximum fault tolerance, but also for the natural way of labeling the processors (vertices), scheme presented previously. As a direct result, this topology allows a constant time addressing (routing) scheme and a linear time algorithm, in terms of the diameter, for one-to-many broadcasting [Chen90].

This section intends to point out that a generalized topology is also possible, a topology which may be useful especially when expanding the network to larger diameters. The optimal case allows only increments of *6d* when updating from diameter *d-1* to *d,* whereas the generalized $T_{i,j}$ allows variable increments, as shown in Table 1. However, the presented topology

has a smaller network expansion increment than many of the well-known topologies.

According to the values of the diameter for various i and j, as shown in Table 1., in order to expand the topology of the network to a different diameter, one could both add or remove nodes in the network.

For example, the network model $T_{7,4}$ has 93 vertices and a diameter of 5. If we reconfigure the topology to $T_{9,1}$, we obtain a network with a higher diameter, 6, but less nodes, 91. Notice also that for the same number of vertices, one could build two different topologies with different diameters, as shown in the above table for $T_{6,5}$ and $T_{9,1}$. In any case, we generate a very rich family of graphs on distinct number of vertices, all with remarkable properties, both topologically and algebraically.

Table 1 Some values of $\rho_{i,j}$ (diameter) for $T_{i,j}$ for various i and j.

i / j	2	3	4	5	6	7	8	9	10
1	7(1)	13(2)	21(3)	31(3)	43(4)	57(5)	73(5)	91(6)	111(7)
2		19(2)	-	39(3)	-	67(5)	-	103(6)	-
3			37(3)	49(4)	-	79(5)	97(6)	-	139(7)
4				61(4)	-	93(5)	-	133(7)	-
5					91(5)	109(6)	129(6)	151(7)	-
6						127(6)	-	-	
7							169(7)	193(8)	219(8)
8								217(8)	-
9									271(9)

A related issue here is the average distance, which for the maximal case, $T_{i,i-1}$ is equal to $(2i-1)/3$. Moreover, since the graph $T_{i,j}$ is 6-connected, the topology possesses a high degree of fault tolerance in terms of connectivity. This implies that the triangulated toroidal network model, as opposed to most of the other existing topologies, can tolerate up to five node and link failures at a time.

Table 2 shows the results for a comparative study among different interconnection topologies, including the regular triangulated toroidal graph (RTT). The optimal mesh refers to a 4-regular triangulated toroidal graph with a maximal number of nodes for a given diameter and which has been introduced in [IrTh99]. As it can be inferred from Table 2, the RTT is more scalable than the hypercube and, moreover, for a network embedded on a surface of genus 1 (torus), the RTT (i.e., $T_{i,i-1}$) has the maximum number of nodes possible for a given diameter and constant node degree 6. There exist

degree 6 network topologies with the same diameter and more nodes but which are not embeddable on a torus surface.

Table 2 Comparison among various multiprocessor architectures.

Parameter Topology	|V| (nodes)	|E| (links)	Diameter	Degree	Connectivity
Clique K_n	p	p(p-1)/2	1	p-1	p
Hypercube Q_n	$p=2^n$	$n2^{n-1}$	n	n	n
Cycle C_n	p	p	[p/2]	2	2
Chordal Ring	p	3p/2	$O(p^{1/2})$	3	3
N1xN2 Mesh	p=N1xN2	2p	$O(p^{1/2})$	4	4
Optimal Mesh	$p=2n^2+2n$	2p	$n = O((p/2)^{1/2})$	4	5
RTT. $T_{i,i-1}$	$p=3n^2+3n+1$	3p	$n = O((p/3)^{1/2})$	6	6

The topology of the generalized $T_{i,j}$ graph becomes very complex for analysis purposes, when i and j are arbitrary numbers with GCD(i,j)=1. This constituted and impediment in finding an efficient routing algorithm for this case. However, based on the translation isomorphism property and the symmetry along the *x*, *y*, and *z* axes, the following formula holds for any given node address (label) *a*.

$$a = x \cdot 1 + y \cdot k + z \cdot (k-1) \quad (6)$$

where *x*, *y* and *z* are the number of hops from the origin to the node labeled a along the three directions. Formula (6) actually determines the minimum number of routing hops between any two nodes (without enumerating the nodes in the route), based on the assumption of vertex-transitivity. That is, given two nodes *s* and *d*, the minimum number of hops between the two nodes (the shortest path) can be determined by solving the following integer problem:

$$\begin{aligned} \text{minimize} \quad & |x| + |y| + |z| \\ \text{such that} \quad & x + yk + z(k-1) = d - s \\ & -d_0 \le x, y, z \le d_0 \end{aligned}$$

where d_0 is the diameter of the maximal $T_{i',i'-1}$ inscribed in $T_{i,j}$ and *k* is the parameter *k* computed earlier.

Given the properties shown earlier in this paper, the graph topology described here is also a Cayley graph based on the cyclic group $< 1, k, k^2, -1, -k, -k^2 >$, with k being the same parameter as above. Cayley graphs are frequently used in modeling and analysis of interconnection networks, due to certain symmetries that the Cayley graph representation manages to emphasize [DiMo96, GrMa64].

5.3 Applications to Cellular Networks

Channel assignment for wireless mobile units is classically modeled by assuming the coverage regions of transceivers ($\mathbf{T}$) partition the plane into disjoint hexagons [Hale80], [Katz96], [MacD79], [Poll96]. The overlap regions, as shown in Figure 14, incidental to the coverage regions being more like circles than hexagons are excluded from the fundamental hexagonal lattice. Overlap regions are separately identified with reference to methods of hand-off, but the size and variation in overlap regions is not easily investigated in this traditional model [Poll96]. Our research included the extensive modeling of various forms of overlap segments and their regularities in a cellular arrangement. A new approach to the channel assignment problem in the presence of extensive overlap between coverage regions was obtained by graph theoretic modeling of the cellular assignment [YaMa97], [Yang91], [MaIr98], [MaIr99] [Irid98].

The strong overlap arrangement of Figure 15b, as opposed to the weak overlap in Figure 15a, suggests a good approximation is simply to have the full triangles of the planar dual triangular lattice serve as the overlap 3-segments, with no other cell segments admitted. The dual triangular lattice, whose vertices are now the transceivers, is shown in Figure 14.

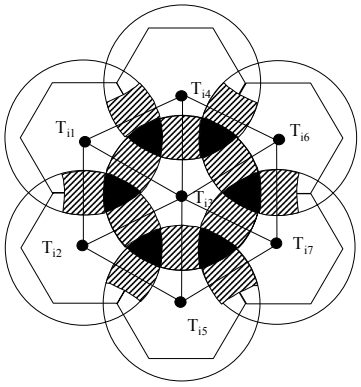

A cluster of k contiguous cells of the hexagonal lattice, where each cell has a distinct one of the k fixed subsets of the available frequency channels, is

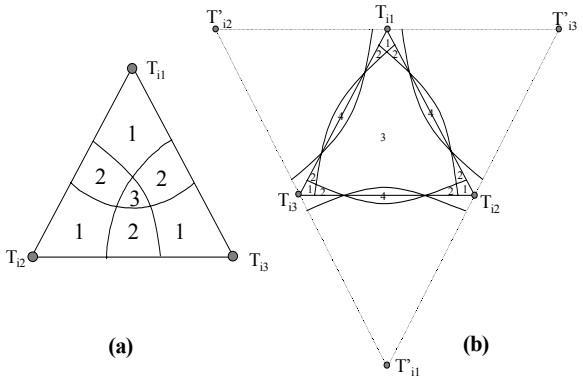

termed a *frequency repeat tile.* A covering of the plane by this frequency repeat tile is termed a *frequency repeat tiling of the plane.*

Frequency repeat patterns typically involve a relatively small number of cells, with $k=7$ often employed for examples in the literature. We shall in general be interested in *m-cell* repeat sample regions for larger values of m that may or may not be related to multiples of the frequency repeat.

Here we focus on the *m-cell* sample region repeats that can be identified with simple polygonal shapes such as a rectangle, rhombus, or hexagon. The 7-cell repeat can be associated with a hexagon providing one important example, but many larger repeats will also be of interest.

For m-cell repeats associated with a rectangle, rhombus, or a hexagon, as shown in Section 2, it follows that the infinite triangular lattice can be homomorphically mapped onto an m-vertex toroidal graph, such that the vertex, edge and face associations with hexagonal cells and overlap regions are preserved. When m is an appropriate multiple of k, the frequency channel set associations are also preserved. For homomorphisms corresponding to k-cell frequency repeats, the relatively small toroidal graph provides a sufficient model for investigating and displaying properties of the frequency channel distribution.

The larger (m-vertex) toroidal graphs, derived from a sample region repeat, provide reasonable sized underlying structures for probabilistic mobile unit channel assignment studies. Theoretically and/or by simulation, channel assignment strategies, blocked regions, call cutoffs, and other probabilistic occurrences at load levels near full capacity, can be realistically studied in the m-vertex toroidal graph model without anomalies due to boundary effects. Loading patterns over multiple cell regions will be quite realistic for estimation of the infinite lattice cellular network, provided the multiple cell regions constitute planar subgraphs of the toroidal graph.

To simulate this cellular system without boundary effects, we take the repeat tile and embed it on a torus [CaIr99]. The toroidal model is a natural and pertinent way of simulating and analyzing the behavior of the infinite cellular network using a finite model. If the repeat tile is a hexagon, constructed as described previously, the toroidal model obtained is the $T_{i,j}$ graph. The Voronoi diagrams technique identifies a cluster of vertices that are closer to a repeat origin point than to any other origin point.

The hexagonal repeat pattern can be easily employed in a multitier system where we can identify two repeat levels:

1. a frequency repeat, relatively small (the $micro\text{-}cell$);
2. a toroidal repeat (the $macro\text{-}cell$).

Different rhombic numbers, as shown in Figure 16, characterize the micro-cell and the macro-cell. The toroidal embedding of the macro-cell will take care of the undesired boundary effect. The shifting parameters for the macro-cell, as shown in Figure 16, are (7,7) and for the micro-cell, they are (2,1). We can also identify the shifting parameters (4,1) for the macro-cell in terms of micro-cell units. It can be easily verified that $4^2+4\cdot1+1^2 = 21$, which is the total number of micro-cells contained in the macro-cell. The total number of transceivers covered by the macro-cell is equal to: $21\text{x}7=7^2 + 7\cdot7+7^2= 147$.

Observation: Any region of triangles, inside a macro-cell, of radius smaller than the macro-cell radius is planar. This follows from the sizes of the diameters of the two types of cells.

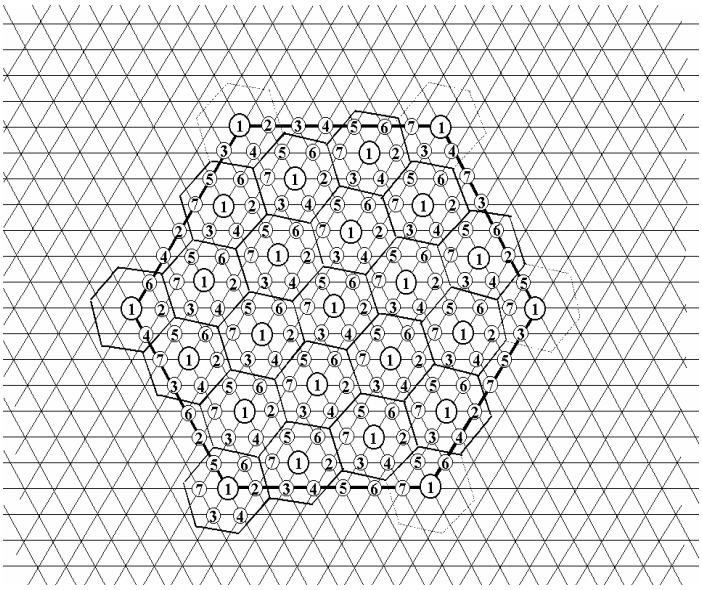

Figure 16 A toroidal embedding hexagonal repeat macro-cell ($T_{7,7}$), containing 21 micro-cells of 7-frequency hexagonal repeats ($T_{2,1}$)

Hence, we can locally study a region within the macro-cell that is reasonably unrelated to the toroidal embedding. Moreover, we can take any contiguous region with the above-specified radius constraint from the toroidal macro-cell, without worrying about being too close to the "boundary" and thus introducing unrealistic behavior.

All the contained micro-cells are similar and their behavior will not be influenced by their position within the macro-cell.

6 Conclusions

In this paper we introduced a 6-regular toroidal graph, constructed from a hexagonal tiling of the infinite triangular lattice. The graph, denoted by $T_{i,j}$, where i, and j are the shifting parameters of the rhombic number $\rho_{i,j,}$ represents a homomorphism of the triangular lattice and has a very symmetric structure. Some of its properties, such as vertex- and edge-transitivity, rotation homomorphism, Hamiltonian cycle decomposition, and coloring, have been presented and discussed. When the shifting parameter j is equal to $i-1$, the graph is optimal, in the sense that it features the largest packing of vertices for a 6-regular graph, embeddable on a surface of genus 1 (locally planar), for a given diameter. The computation of the diameter of the graph involves computational geometry tools and is also presented in this paper.

Due to its highly symmetric topology, the $T_{i,j}$ graph family, and especially the optimal case, $T_{i,i-1}$, has a series of applications in modeling and analysis of networks. In this paper we presented two of its applications, more specific, in interconnection and cellular networks. In interconnection networks, where one of the demands is to design topologies that feature high connectivity and fault tolerance, the optimal $T_{i,i-1}$ represents a very attractive topology, which is also characterized by a constant time routing scheme, due to the natural labeling scheme presented here.

In cellular networks, the graph is used to model and simulate without boundary artifacts, cellular assignment in systems with extensive overlap of transceiver coverage regions. The $T_{i,j}$ graph is employed in the modeling of micro- and macro-cell systems and it offers a systematic labeling scheme useful for frequency planning.

References

[Arna80] J.-F. Arnaud, *Frequency Planning in Europe*, IEEE Proc., Vol. 68, No. 12, Dec 1980

[Aker89] B. Akers, B. Krishnamurthy, *A Group Theoretic Model for Symmetric Interconnection Networks*, IEEE Transactions on Computers, Vol. 38, No. 4, pp. 555-566, 1989

[BaeB97] M. M. Bae, B. Bose, *Resource Placement in Torus-Based Networks*, IEEE Transactions on Computers, Vol. 46, No. 10, Oct. 1997

[Bhuy97] L. N. Bhuyan, X. Zhang, Tutorial on Multiprocessor Performance Measurement and Evaluation, IEEE CS Press, 1997

[Boll79] B. Bollobas, *Graph Theory: An Introductory Course*, N. Y. Springer-Verlag, 1979

[BoEr76] B. Bollobas, P. Erdos, *Alternating Hamiltonian Cycles*, Israel J. Math., 23(1976)

[Broo41] R. L. Brooks, *On colouring the nodes of a network*, Proceedings Cambridge Phil. Soc. 37, pp. 194-197, 1941

[CaIr99] H. C. Cankaya, M. Iridon, D. W. Matula, *Performance Analysis of a Graph Model for Channel Assignment in a Cellular Network*, COMPSAC 1999

[Chen90] M. S. Chen, K. G. Shin, *Addressing, Routing, and Broadcasting in Hexagonal Mesh Multiprocessors*, IEEE Transactions on Computers, Vol. 39, No. 1, Jan. 1990

[Chva85] V. Chvatal, *Hamiltonian Cycles*, John Wiley & Sons Ltd., 1985

[ChEr72] V. Chvatal, P. Erdos, *A note on Hamiltonian circuits*, Discrete Math, 2(1972)

[DiMo96] J. Dixon, B. Mortimer, *Permutation Groups*, New York, Springer Verlag, 1996

[FoFu62] L. R. Ford, Jr., D. R. Fulkerson, *Flows in Networks*, Princeton Univ. Press, 1962

[Fort92] S. Fortune, *Voronoi Diagrams and Delauny Triangulations*, edited by D.-Z. Du and F. Hwang, Computing in Euclidean Geometry, Vol. 1, pp 193-234, World Scientific, 1992

[GrMa64] I. Grossman, W. Magnus, *Groups and Their Graphs*, New York Random House, 1964

[Hale80] J. Hale, *Frequency Assignment*, IEEE Proc., vol. 68, no. 12, Dec. 1980

[Hara72] F. Harary - *Graph Theory*, Addison-Wesley, 1972

[HaWr79] G. H. Hardy, E. M. Wright, *An Introduction to the Theory of Numbers*, Clarendon Press, Oxford, 1979

[Heyd97a] M.-C. Heydemann, N. Marlin, S. Perennes, *Cayley Graphs with Complete Rotations*, Research Report: INRIA 3624, 1997

[Heyd97b] M.-C. Heydemann, *Cayley Graphs and Interconnection Networks*, Proceedings Graph Symmetry, Montreal, 1996, NATO ASI C, 1997

[Irid98] M. Iridon, D. W. Matula, *Symmetric Cellular Network Embeddings on a Torus*, IEEE Proc. ICCCN, 1998, pp. 732-736

[IrTh99] M. Iridon, Regular Triangulated Toroidal Graphs with Applications in Cellular and Interconnection Networks, Ph.D. Thesis, Southern Methodist University, May 1999

[Katz96] I. Katzela, M. Nagshineh, Channel Assignment Schemes for Cellular Mobile Telecommunication Systems: A Comprehensive Survey, IEEE Personal Communications, June 1996

[KoMa85] P. Kornerup, D. W. Matula, *Finite Precision Lexicographic Continued Fraction Number Systems*, IEEE Proc. 7th Symposium on Computer Arithmetic, June 1985

[MacD79] V.H. MacDonald, *The Cellular Concept*, The BELL System Technical Journal, Jan 1979, Vol. 58, No. 1, p.15-41

[MaIr98] D. W. Matula, M. Iridon, C. Yang, H. C. Cankaya, *A Graph Theoretic Approach for Channel Assignment in Cellular Networks*, 2nd International Workshop on Discrete Algorithms and Methods for Mobile Computing and Communications, Dallas, Oct. 1998. In conjunction with ACM/IEEE Mobicom'98

[MaIr99] D. W. Matula, M. Iridon, C. Yang, *A Graph Theoretic Approach for Channel Assignment in Cellular Networks*, Wireless Networks Journal, Vol. 7, 2001, pp. 567-574

[MaKo80] D. W. Matula, P. Kornerup, *Formulations of Finite Precision Rational Arithmetic*, Springer Verlag, 1980

[Mold93] I.D. Moldovan, *Parallel Processing - From Systems to Applications*, Morgan Kaufmann Publishers, 1993

[Poll96] G. P. Pollini, *Trends in Handover Design*, IEEE Communications Magazine, March 1996

[Sieg96] H. J. Siegel, C. B. Stunkel; *Inside Parallel Computers: Trends in Interconnection Networks*, IEEE CS&E, Vol. 3, No 3, Fall 1996, pp. 69-71

[SiKa94] J. F. Sibeyn, M. Kaufmann, *Deterministic l-k Routing on Meshes*, STACS 1994, pp. 237-248

[Thom80] C. Thomassen, *Hamiltonian-connected Tournaments*, Journal of Combinatorial Theory, B 28(1980).

[Till80] T. W. Tillson, *Hamiltonian Decomposition of* $K^*_{2m}, 2m \geq 8$, Journal of Combinatorial Theory, Ser. B, 29(1980).

[West96] D. B. West, *Introduction to Graph Theory*, Prentice Hall, 1996

[YaMa97] C. Yang, D. W. Matula, A Multi-layered Arrangement for Load Sharing in a Cellular Communication System, U.S. Patent #5,633,915, May 1997.

[Yang90] C. Yang, A Multi-Layer Design and Load Sharing Algorithm for Personal Communication Networks, Ph.D. Thesis, Aug. 1991